ORIGINAL ARTICLE

Journal of Cachexia, Sarcopenia and Muscle 2022; **13**: 713–727
Published online 24 November 2021 in Wiley Online Library (wileyonlinelibrary.com) **DOI:** 10.1002/jcsm.12867

Sepsis induces interleukin 6, gp130/JAK2/STAT3, and muscle wasting

Lukas Zanders[1,2,3], Melanie Kny[1], Alexander Hahn[1], Sibylle Schmidt[1], Sebastian Wundersitz[1], Mihail Todiras[4,5], Ines Lahmann[6], Arnab Bandyopadhyay[7], Tobias Wollersheim[8,9], Lars Kaderali[7,10], Friedrich C. Luft[1], Carmen Birchmeier[6,9], Steffen Weber-Carstens[8,9] & Jens Fielitz[1,9,10,11]*

[1]*Experimental and Clinical Research Center (ECRC), Charité-Universitätsmedizin Berlin, Max Delbrück Center for Molecular Medicine in the Helmholtz Association (MDC), Berlin, Germany;* [2]*DZHK (German Center for Cardiovascular Research), partner site Berlin, Berlin, Germany;* [3]*Department of Cardiology, Charité Campus Benjamin Franklin, Berlin, Germany;* [4]*Cardiovascular hormones, Max Delbrück Center (MDC) for Molecular Medicine in the Helmholtz Association, Berlin, Germany;* [5]*Nicolae Testemiţanu State University of Medicine and Pharmacy, Chişinău, Moldova;* [6]*Developmental Biology/Signal Transduction, Max-Delbrück-Center for Molecular Medicine, Berlin, Germany;* [7]*Institute of Bioinformatics, University Medicine Greifswald, Greifswald, Germany;* [8]*Anesthesiology and operative Intensive Care Medicine, Charité Campus Virchow and Campus Mitte, Berlin, Germany;* [9]*Berlin Institute of Health (BIH), Berlin, Germany;* [10]*DZHK (German Center for Cardiovascular Research), partner site Greifswald, Greifswald, Germany;* [11]*Department of Internal Medicine B, Cardiology, University Medicine Greifswald, Greifswald, Germany*

Abstract

Background Sepsis and inflammation can cause intensive care unit-acquired weakness (ICUAW). Increased interleukin-6 (IL-6) plasma levels are a risk factor for ICUAW. IL-6 signalling involves the glycoprotein 130 (gp130) receptor and the JAK/STAT-pathway, but its role in sepsis-induced muscle wasting is uncertain. In a clinical observational study, we found that the IL-6 target gene, *SOCS3*, was increased in skeletal muscle of ICUAW patients indicative for JAK/STAT-pathway activation. We tested the hypothesis that the IL-6/gp130-pathway mediates ICUAW muscle atrophy.

Methods We sequenced RNA (RNAseq) from tibialis anterior (TA) muscle of cecal ligation and puncture-operated (CLP) and sham-operated wildtype (WT) mice. The effects of the IL-6/gp130/JAK2/STAT3-pathway were investigated by analysing the atrophy phenotype, gene expression, and protein contents of C2C12 myotubes. Mice lacking *Il6st*, encoding gp130, in myocytes (cKO) and WT controls, as well as mice treated with the JAK2 inhibitor AG490 or vehicle were exposed to CLP or sham surgery for 24 or 96 h.

Results Analyses of differentially expressed genes in RNAseq (≥2-log2-fold change, $P < 0.01$) revealed an activation of IL-6-signalling and JAK/STAT-signalling pathways in muscle of septic mice, which occurred after 24 h and lasted at least for 96 h during sepsis. IL-6 treatment of C2C12 myotubes induced STAT3 phosphorylation (three-fold, $P < 0.01$) and *Socs3* mRNA expression (3.1-fold, $P < 0.01$) and caused myotube atrophy. Knockdown of *Il6st* diminished IL-6-induced STAT3 phosphorylation (−30.0%; $P < 0.01$), *Socs3* mRNA expression, and myotube atrophy. JAK2 (− 29.0%; $P < 0.01$) or STAT3 inhibition (−38.7%; $P < 0.05$) decreased IL-6-induced *Socs3* mRNA expression. Treatment with either inhibitor attenuated myotube atrophy in response to IL-6. CLP-operated septic mice showed an increased STAT3 phosphorylation and *Socs3* mRNA expression in TA muscle, which was reduced in septic *Il6st*-cKO mice by 67.8% ($P < 0.05$) and 85.6% ($P < 0.001$), respectively. CLP caused a loss of TA muscle weight, which was attenuated in *Il6st*-cKO mice (WT: −22.3%, $P < 0.001$, cKO: −13.5%, $P < 0.001$; WT vs. cKO $P < 0.001$). While loss of *Il6st* resulted in a reduction of MuRF1 protein contents, Atrogin-1 remained unchanged between septic WT and cKO mice. mRNA expression of *Trim63*/MuRF1 and *Fbxo32*/Atrogin-1 were unaltered between CLP-treated WT and cKO mice. AG490 treatment reduced STAT3 phosphorylation (−22.2%, $P < 0.05$) and attenuated TA muscle atrophy in septic mice (29.6% relative reduction of muscle weight loss, $P < 0.05$). The reduction in muscle atrophy was accompanied by a reduction in *Fbxo32*/Atrogin-1-mRNA (−81.3%, $P < 0.05$) and *Trim63*/MuRF1-mRNA expression (−77.6%, $P < 0.05$) and protein content.

Conclusions IL-6 via the gp130/JAK2/STAT3-pathway mediates sepsis-induced muscle atrophy possibly contributing to ICUAW.

Keywords gp130; IL-6 signalling; Inflammation; Sepsis; Muscle atrophy; Intensive care unit acquired weakness

Received: 1 July 2021; Revised: 18 October 2021; Accepted: 20 October 2021
**Correspondence to: Jens Fielitz, Universitätsmedizin Greifswald, Klinik und Poliklinik für Innere Medizin B Forschungscluster III, Fleischmannstr. 41, 17475 Greifswald, Germany. Phone: +49 3834 86 80519; Fax: +49 3834 86 80502. Email: jens.fielitz@uni-greifswald.de*

Introduction

Intensive care unit-acquired weakness (ICUAW) affects up to 90% of patients with severe sepsis increasing their morbidity and mortality.[1,2] ICUAW is characterized by a loss of muscle mass, a reduction in myofibre size, and a decreased muscle strength leading to persisting physical impairment.[3] This phenotype results from a dysregulated protein homeostasis with increased protein degradation and decreased protein synthesis, eventually causing a decrease of muscle structural proteins.[4,5] In ICUAW, atrophy predominantly occurs in fast twitch/type II myofibres[6] and is mainly mediated by the ubiquitin-proteasome system. The E3 ligase muscle RING-finger protein-1 (MuRF1), encoded by *Trim63*, and the F-Box protein Atrogin-1, encoded by *Fbxo32*, are key factors for ubiquitin-proteasome system-mediated protein degradation in muscle atrophy.[7] Both MuRF1 and Atrogin-1 are increased early and persistently during critical illness and possibly mediate muscle atrophy in ICUAW patients.[4,6] Inflammation and sepsis are major risk factors for ICUAW.[8,9] Previously, we reported that interleukin 1β (IL-1β)[10] and the acute-phase protein serum amyloid A1 (SAA1)[11,12] promote muscle atrophy in sepsis, and that their inhibition attenuated sepsis-induced muscle atrophy in mice. Both IL-1β and SAA1 signalling converge on the transcription factor NF-κB (nuclear factor 'kappa-light-chain-enhancer' of activated B-cells) and increase the expression of interleukin 6 (IL-6).[10–12] IL-6 regulates protein homeostasis in the skeletal muscle.[13,14] While an acute increase in systemic IL-6 promotes muscle growth and hypertrophy, its sustained elevation, as occurring in cancer or diabetes, causes muscle atrophy.[15,16] However, the role of IL-6 signalling in sepsis-induced muscle atrophy is not well understood.

IL-6 can signal through the canonical pathway, where IL-6 binds to its α-receptor (IL-6R) on the cell surface, and induces homodimerization and association with the signal transducing β-receptor glycoprotein 130 (gp130, encoded by *Il6st*). Alternatively, IL-6 can use the trans-signalling pathway, where it binds to a soluble IL-6R, which associates with gp130. In both pathways, the activated IL-6R-gp130 complex binds and activates the Janus kinase (JAK) family of tyrosine kinases, primarily JAK1, JAK2, and TYK2, which phosphorylate the cytoplasmatic tail of gp130, enabling the association of the Signal Transducer and Activator of Transcription (STAT), mainly STAT1 and STAT3. Phosphorylated STAT (i.e. STAT3 Y705) proteins dimerize and translocate to the nucleus where they control the expression of their target genes, such as Suppressor of Cytokine Signalling 3 (*SOCS3*).[17,18] SOCS3 acts as a negative feedback inhibitor of cytokine signalling by inhibition of JAK1, JAK2, and Tyk2.[19] *In vitro*, SOCS3 also inhibits the Insulin/PI3K/Akt pathway as a substrate recognition component of an E3 ubiquitin ligase complex, degrading Insulin Receptor Substrate 1 (IRS-1) that is essential for insulin signalling.[20] Insulin increases protein synthesis[21] and decreases atrogene expression and protein degradation[22] via the PI3K/Akt pathway in mice. This promotes muscle growth and inversely perturbations can aggravate muscle atrophy that is frequently seen in critically ill patients.[23] Based on these data and together with our observation that increased IL-6 plasma level is a risk factor for Critical Illness Myopathy (CIM) in patients,[8] we hypothesized that the IL-6/gp130/JAK/STAT pathway plays a role in sepsis-induced muscle atrophy.

Methods

Patient samples

The institutional review board of the *Charité Universitätsmedizin Berlin*, Germany, approved the study, and written informed consent was obtained from legal proxy [intensive care unit (ICU) patients], or the patients themselves before inclusion in the study (*Charité* EA2/061/06; http://www.controlled-trials.com, ISRCTN77569430). Clinical data were reported previously.[11] We analysed mRNA expression in biopsy specimens obtained from the *vastus lateralis* muscle of patients at high risk to develop ICUAW. Accordingly, these patients (n = 5) were critically ill, mechanically ventilated with a SOFA score ≥8 on three consecutive days within the first 5 days after ICU admission. Biopsy specimens were taken at Day 5 and Day 15 after ICU admission. Five age-matched and gender-matched patients undergoing elective orthopaedic surgery permitted muscle biopsies and were used as controls. For more details on the clinical data, please refer to Wollersheim *et al*. and Langhans *et al*.[4,11]

Animal model of polymicrobial sepsis

All animal procedures were performed in accordance with the guidelines of the Max-Delbrück Center for Molecular Medicine and the *Charité-Universitätsmedizin Berlin*, and were approved by the *Landesamt für Gesundheit und Soziales* (LAGeSo, Berlin, Germany; permit number G 207/13). The investigation conforms to the *Guide for the Care and Use of Laboratory Animals* published by the US National Institutes of Health (NIH Publication No. 85-23, revised 1985), as well as the current version of German Law on the Protection of Animals.

Klaus Rajewsky kindly provided conditional *Il6st* knockout (KO) mice.[24] *Il6st*$^{loxP/loxP}$ mice were crossed with Cre carrying mice controlled by myoblast-specific Pax7-promotor (Pax7-Cre) (cKO, Il6st$^{loxP/loxP;\ Pax7\text{-}Cre}$). Pax7-Cre-negative littermates were used as controls (WT, *Il6st*$^{loxP/loxP}$). Genotyping was performed as recently described[10] using primer pairs shown in *Supporting information Table* S1.

Cecal ligation and puncture (CLP) surgery was performed in 12- to 16-week-old male *Il6st c*KO mice and WT littermate controls, as recently described.[10,25] Sham mice were treated identically except for the ligation and puncture of the cecum. The effects of AG490 treatment on sepsis-induced muscle atrophy were investigated in 20-week-old male C57BL/6J mice. Animals received vehicle (10 μL DMSO in 240 μL normal saline) or AG490 (16 mg/kg in 250 μL vehicle) 60 min prior to, and every 24 h after surgery for 96 h.

Mice were sacrificed 24 or 96 h after surgery, as indicated, and *tibialis anterior* (TA) and *gastrocnemius/plantaris* (GP) muscles were harvested for analysis. Body, muscle, and organ weight was measured and normalized to tibia length. Measurements of plasma IL-6 were performed using the Mouse ELISA Quantikine Kit for IL-6 (R&D Systems, MN, USA) according to the manufacturers' protocol.

RNA sequencing and statistical analyses

Three biological replicates of WT sham and WT CLP 24 and 96 h after surgery were sequenced. Total RNA analyses were evaluated by an Agilent 2100 Bioanalyzer (Agilent Technologies, Inc., CA, USA). Library preparation of 500 ng RNA was performed using the Illumina TruSeq Stranded mRNA Kit. cDNA was evaluated and sequencing was performed using an Illumina HiSeq 4000 sequencer. The transcriptome data can be found under EBI Annotare v.2.0 (E-MTAB-10960). Pathway enrichment analysis was performed using DAVID (Database for Annotation, Visualization and Integrated Discovery) Bioinformatics Resources 6.8 (https://david.ncifcrf.gov) using the outputs BP_ALL (all biological process terms). For further information, please refer to the supporting information.

Histological analyses

Tibialis anterior and *gastrocnemius/plantaris* muscles were flash frozen in liquid nitrogen with gum tragacanth (Merck KGaA, Germany), cut with a thickness of 5 μm and stained with metachromatic ATPase. One hundred myocyte cross-sectional areas (MCSAs) were measured per mouse, muscle and condition in a blinded fashion.

Myoblast culture, differentiation, and atrophy assay

Cell culture experiments were performed in 5 days differentiated C2C12 cells (American Type Culture Collection, Manassas, VA, USA). Myocytes were treated with 10 ng/mL of recombinant IL-6 (R&D Systems, MN, USA) or solvent (0.1% bovine serum albumin in phosphate-buffered saline) for the indicated times. The JAK2 inhibitor AG490 (10 μM, Sigma-Aldrich, MO, USA), and two STAT3 inhibitors (C188-9; 10 μM, Merck-Millipore, Germany; S3i-201, 10 μM, Selleckchem) were added 60 min prior to IL-6 treatment. For siRNA transfection we used the Dharmacon SmartPool siRNA targeting Il6st (J-040007-09-0005, Dharmacon/Fisher Scientific; control siRNA D-001810-10-05). Transfection was performed as per the manufacturer's protocol. Light microscopy pictures were analysed using the Leica CTR 6500 microscope and the Leica DFC 360 FX digital camera. Out of 100 myotubes per condition, three diameters per myotube were measured and averaged using the ImageJ software in a blinded fashion.

RNA isolation, cDNA synthesis, and quantitative real-time-polymerase chain reaction

RNA isolation was performed using TRIzol® Reagent (Invitrogen™, Life Technologies Corporation, CA, USA) and the FastPrep-24™ instrument (MP Biomedicals GmbH). SuperScript® First-Strand Synthesis System (Invitrogen™, Life Technologies Corporation, CA, USA) was used for cDNA synthesis. Quantitative real-time polymerase chain reaction (qRT-PCR) was performed using *Power* SYBR® Green PCR Master Mix (Thermo Fischer Scientific Inc., MA, USA) and self-designed primers (for primer sequences, refer to *Table* S2). PCR reactions were performed in a StepOnePlus™ thermocycler (Applied Biosystems). Gene expression was normalized to glyceraldehyde-3-phosphate dehydrogenase (*Gapdh*).

Protein extraction and Western blot assay

Muscle tissue was homogenized in lysis buffer using the FastPrep-24™ instrument. Lysates were separated by

SDS-PAGE and transferred to PVDF or nitrocellulose membranes (GE Healthcare, Germany). Membranes were incubated with the indicated primary and secondary antibodies. The antibodies used are indicated in the supporting information. GAPDH was used as loading control. We used the SuperSignal® West Pico Chemiluminescent substrate (Thermo Fischer Scientific Inc., MA, USA) and Chemiluminescence detection films (GE Amersham, UK) for protein visualization.

Statistics

All experiments were performed independently and at least three times using biological triplicates each. For mRNA expression, myotube diameter and MCSA data from cell culture experiments, a paired *t* test was used. Data on muscle weight and mRNA expression were analysed using the Mann–Whitney *U* test. *In vitro* data are shown as mean ± SD and *in vivo* data are mean ± SEM. Frequency-distribution histograms plotting myotube width or MCSA against its frequency. Differences were considered statistically significant at $P \leq 0.05$. The GraphPad Prism® 8 program (GraphPad Software, La Jolla, CA, USA), Adobe Illustrator CS6, version 16.0.0, and Photoshop CS6, version 13.0 were used to perform statistics and draw graphics, respectively.

Results

Interleukin 6 signalling is activated in skeletal muscle during sepsis

We analysed *SOCS3* mRNA expression in muscle biopsy specimens of ICUAW patients and control subjects. qRT-PCR analysis showed an increased *SOCS3* mRNA expression in the vastus lateralis of critically ill patients at day five and day 15 after ICU-admission compared to controls (*Figure* 1A) indicative for an activation of the IL-6/JAK/STAT pathway.

To confirm that the IL-6/JAK/STAT pathway is activated in muscle during sepsis, we performed next generation sequencing of RNAs (RNAseq) isolated from TA muscles of CLP and sham operated WT mice and analysed these data for changes in the expression of the IL-6 cytokine family and its receptors. *Il6*, *Il6st*, and *Il6ra* expression was significantly increased in muscle after 24 and 96 h of sepsis, whereas the other IL-6 family members showed only minor changes (i.e. *Ctf1* and *Cntf*) or a reduction of gene expression (i.e. *Lif* and *Lifr*) (*Figure* 1B). Analyses of all differentially expressed genes (DEG; ≥2-log2-fold change, adjusted *P* value <0.01) by Voronoi plots showed an enrichment of IL-6 and IL-6 related genes after 24 h, which was even more pronounced after 96 h of sepsis (*Figure* 1C, *Figure* S1). These data show that IL-6 signalling is activated in the TA muscle of septic mice.

Further, gene ontology (GO) term analysis (biological process) revealed a significant enrichment of genes belonging to transcription, translation, autophagy, and proteasomal protein degradation and a decrease in genes involved in TGFβ-signalling and skeletal system development after 24 but not 96 h (*Figure* S2). Kyoto Encyclopedia of Genes and Genomes (KEGG)-pathway analysis showed that insulin resistance and tumour necrosis factor-signalling were increased and TGFβ and insulin signalling were decreased after 24 h but not 96 h (*Figure* S2). Next, we defined a subgroup encompassing 1036 genes that were up-regulated (*Figure* 1D) and 1621 genes that were down-regulated at both time points in sepsis (*Figure* S3). GO term analysis of up-regulated DEG showed an enrichment of ubiquitin-dependent protein degradation. In accordance with our previous data,[10,11] we found an increase in cellular response to IL-1 and acute-phase response, as well as IL-6 signalling and positive regulation of JAK/STAT signalling. KEGG pathway analysis revealed an increase in DEG involved in proteasomal protein degradation, TNF-signalling and JAK/STAT-signalling, and insulin resistance (*Figure* 1D). A strong deregulation of DEG contained in 'cellular response to IL6' (GO:0071354) (*Figure* 1E), 'IL-6 production' (GO:0032635) (*Figure* S4), and 'receptor signalling pathway via JAK-STAT' (GO:0007259) (*Figure* S5) indicated an activation of IL-6 signalling in muscle of septic mice after 24 and 96 h. Collectively, our data indicate that the IL-6 and JAK/STAT pathways are activated in muscle of septic mice after 24 and 96 h.

Interleukin 6 induces atrophy via the gp130/JAK/STAT pathway in C2C12 myotubes

To analyse IL-6 signalling in myocytes, we treated differentiated murine C2C12 myotubes with recombinant IL-6 or solvent. Western blot analysis showed an increased STAT3 Y705 phosphorylation after 5 to 60 min of IL-6 treatment (*Figure* 2A). qRT-PCR revealed that IL-6 increased *Socs3* mRNA expression after 24 to 72 h (*Figure* 2B). IL-6 induced a reduction in myotube diameter by 11.1%, 9.7%, and 7.1% at 24, 48, and 72 h, respectively (*Figure* 2C and 2D). These data indicate that IL-6 activates the JAK/STAT3 pathway and causes atrophy of myocytes *in vitro*.

We next reduced gp130, encoded by *Il6st*, by siRNA prior to IL-6 treatment in C2C12 myotubes. Knockdown was confirmed by qRT-PCR (relative reduction 69%, $P < 0.005$; *Figure* 3A) and immunoblotting (*Figure* 3B). Knockdown of *Il6st* attenuated IL-6-induced STAT3 Y705 phosphorylation (*Figure* 3B), *Socs3* expression (*Figure* 3C) and IL-6-mediated reduction of myotube diameters compared to siRNA controls (8.3% vs. 28.3%, $P < 0.01$; *Figure* 3D). C2C12 myotubes were treated with the JAK2 inhibitor AG490 or the STAT3 inhibitor C188-9 prior to IL-6 treatment. Both inhibitors attenuated IL-6-induced STAT3 Y705 phosphorylation (*Figure* 3E) and *Socs3*

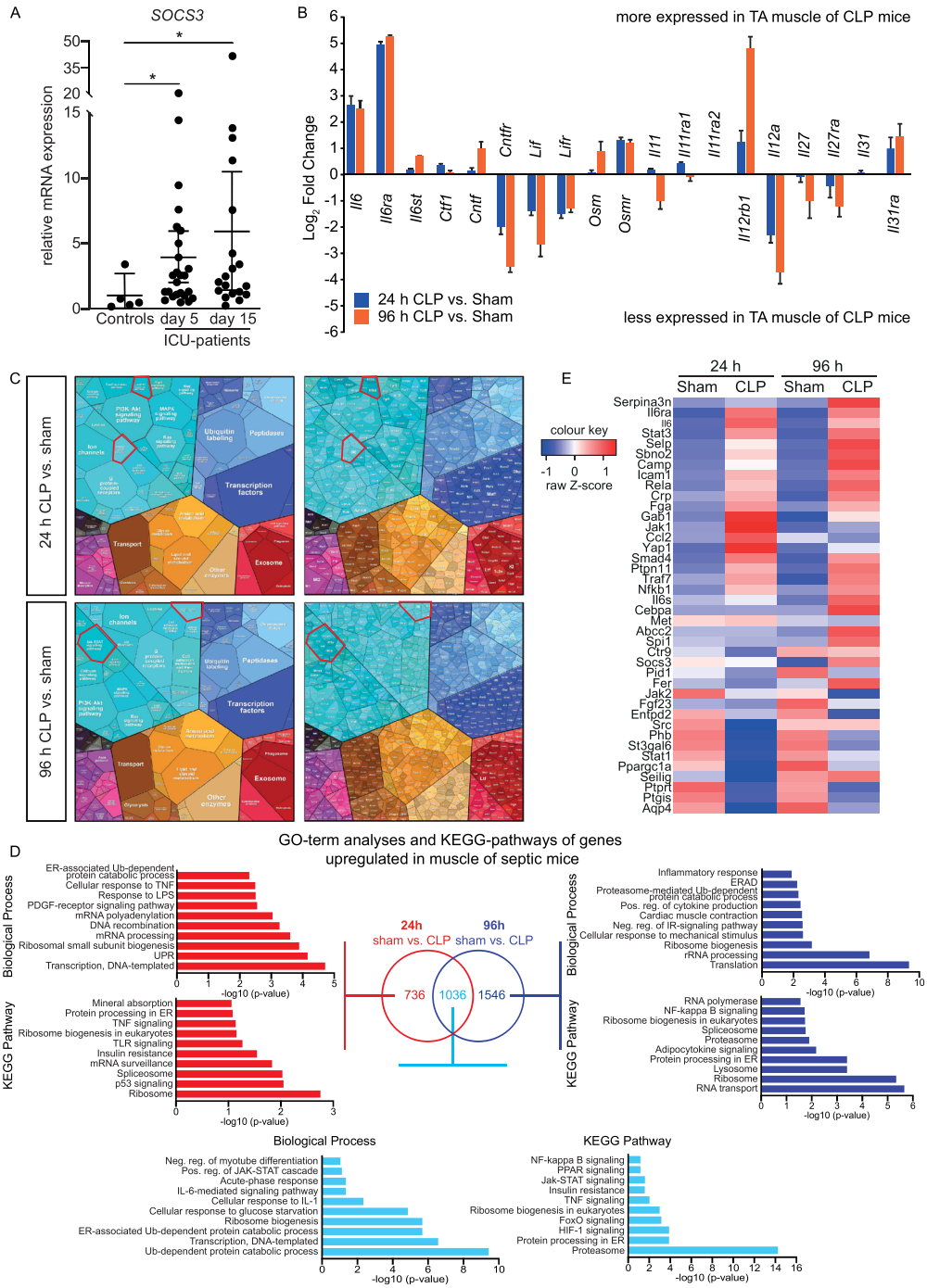

Figure 1 The IL-6 pathway is activated in skeletal muscle during sepsis. (*A*) *SOCS3* mRNA expression in muscle of critically ill patients. Muscle biopsy specimens from critically ill patients were obtained from the *vastus lateralis* muscle on Day 5 (n = 25) and Day 15 (n = 19) in intensive care unit (ICU). Healthy individuals (n = 5) served as controls. Data are presented as fold change (mean ± SEM). *$P < 0.05$. (*B–E*) WT mice were subjected to cecal ligation and puncture (CLP) or sham surgery. RNA sequencing analyses were performed 24 and 96 h after surgery (WT sham, n = 3; WT CLP, n = 3, for both time points). (*B*) Gene expression of known IL6-family members and their receptors in TA muscle of sham- and CLP-operated mice after 24 and 96 h. (*C*) Voronoi plot of differentially expressed genes (log2 fold change≥2, adjusted P value <0.05) from RNA sequencing analysis is shown. Voronoi-plots show the respective GO terms (left panels) and the enriched genes (right panel) per time point (top panels 24 h, bottom panels 96 h) as indicated. Insets localize IL-6- and JAK/STAT pathway. (*D*) Venn diagram showing the number of genes that were increased (log2 fold change≥2, adjusted P value <0.01) in the tibialis anterior muscle compared with sham treated mice after 24 h, 96 h or at both time points. The DAVID functional annotation tool was used for gene ontology (GO) term-pathway and Kyoto Encyclopedia of Genes and Genomes (KEGG)-pathway analyses of each individual time point, and 10 of the most enriched biological processes and pathways are shown. (*E*) Heat map of genes contained in GO-term 0071354 cellular response to IL-6 that were significantly regulated (P value <0.05) in TA muscle of septic mice 24 and 96 h after surgery when compared to TA of sham operated mice.

DOI: 10.1002/jcsm.12867

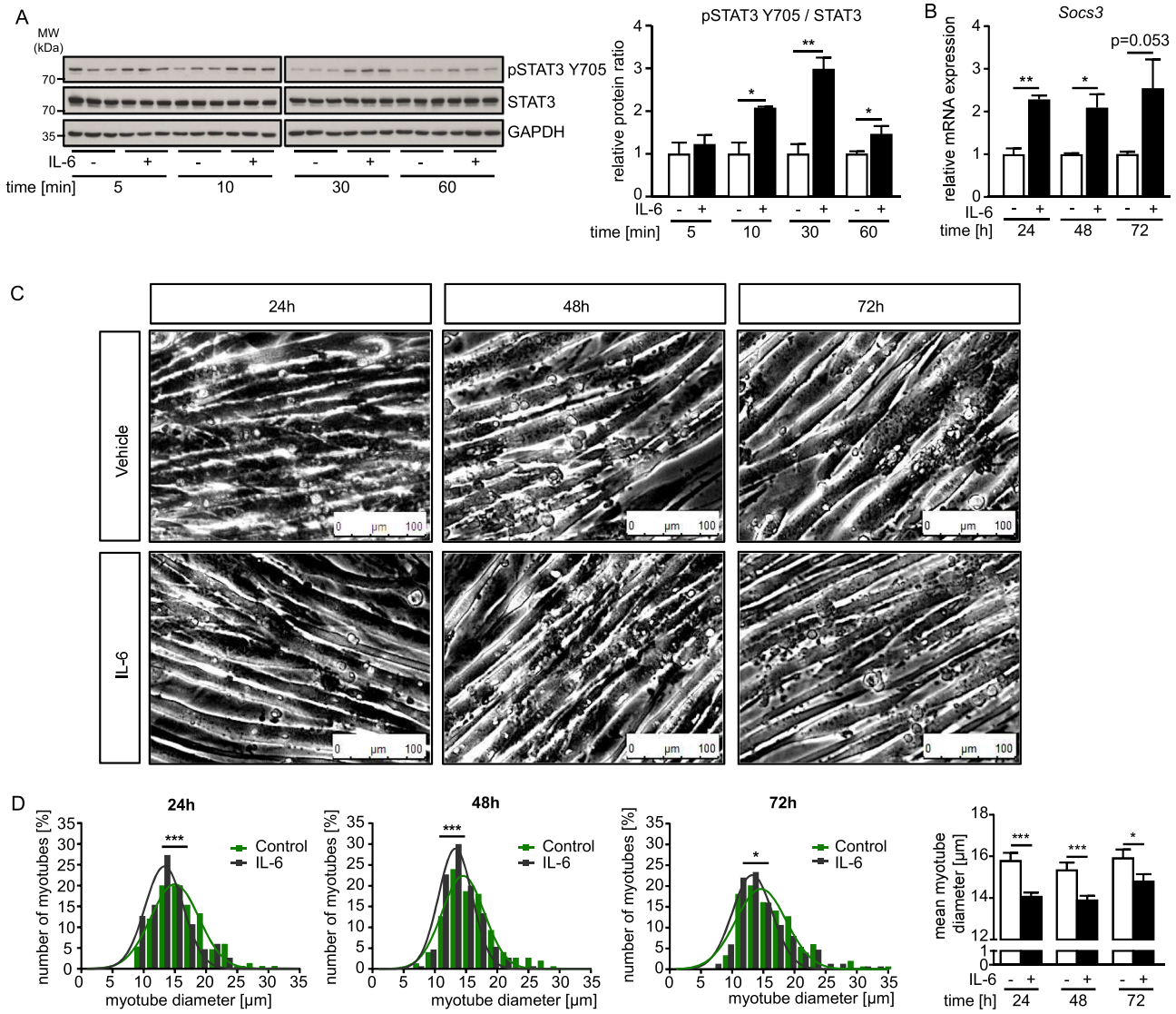

Figure 2 Interleukin 6 activates the JAK/STAT signalling pathway and induces atrophy in myocytes. Five days differentiated C2C12 myotubes were treated with interleukin 6 (IL-6, 10 ng/mL, *n* = 3) or solvent control (0.1% bovine serum albumin in phosphate-buffered saline, *n* = 3) for the indicated time points. (*A*) Western blot analysis with anti-phospho-STAT3-Tyr705 (pSTAT3 Y705), anti-STAT3 and anti-GAPDH antibodies, *n* = 3. GAPDH was used as loading control. Bar graph showing the ratio of the relative densities of pSTAT3 Y705 and STAT3 protein contents as detected C. (*B*) Quantitative real-time polymerase chain reaction (qRT-PCR) analysis of *Socs3* expression. mRNA expression was normalized to *Gapdh*. Data are presented as mean ± SD. $*P < 0.05$, $**P < 0.01$, $***P < 0.001$. MW, molecular weight; min, minutes; IL-6, interleukin 6. (*C*) Representative light microscopy pictures. Scale bar = 100 µm. (*D*) Frequency distribution histograms of cell width of IL-6 and solvent treated myotubes, *n* = 100 cells per condition. Mean myotube width.

expression (*Figure* 3F). IL-6-induced atrophy was attenuated by AG490, C188-9, and S3i-201 (*Figure*s 3G, 3H and S6). These findings reveal that the gp130/JAK2/STAT3 pathway mediates IL-6-induced myotube atrophy.

Skeletal muscle specific deletion of Il6st attenuates sepsis-induced muscle atrophy in mice

To verify our data *in vivo*, we generated mice deficient in *Il6st* in the myocyte lineage. Mice bearing a conditional *Il6st*$^{loxP/loxP}$ allele were bred with mice expressing the Cre-recombinase under the control of the Pax7 promoter (*Il6st*$^{loxP/loxP//Pax7Cre}$, cKO). *Il6st*$^{loxP/loxP}$ littermates not expressing Pax7-Cre served as controls (WT). We performed CLP surgery to induce polymicrobial sepsis for 24 h (to analyse gp130 signalling; WT: *n* = 6; cKO: *n* = 4) and 96 h (to analyse muscle atrophy; WT: *n* = 15; cKO: *n* = 10). Sham operated littermates (24 h: WT: *n* = 4; cKO: *n* = 4; 96 h: WT: *n* = 6; cKO: *n* = 6) served as controls. qRT-PCR analysis confirmed *Il6st* deletion in TA of cKO mice (*Figure* S7A). At baseline, cKO mice showed no differences in survival, body

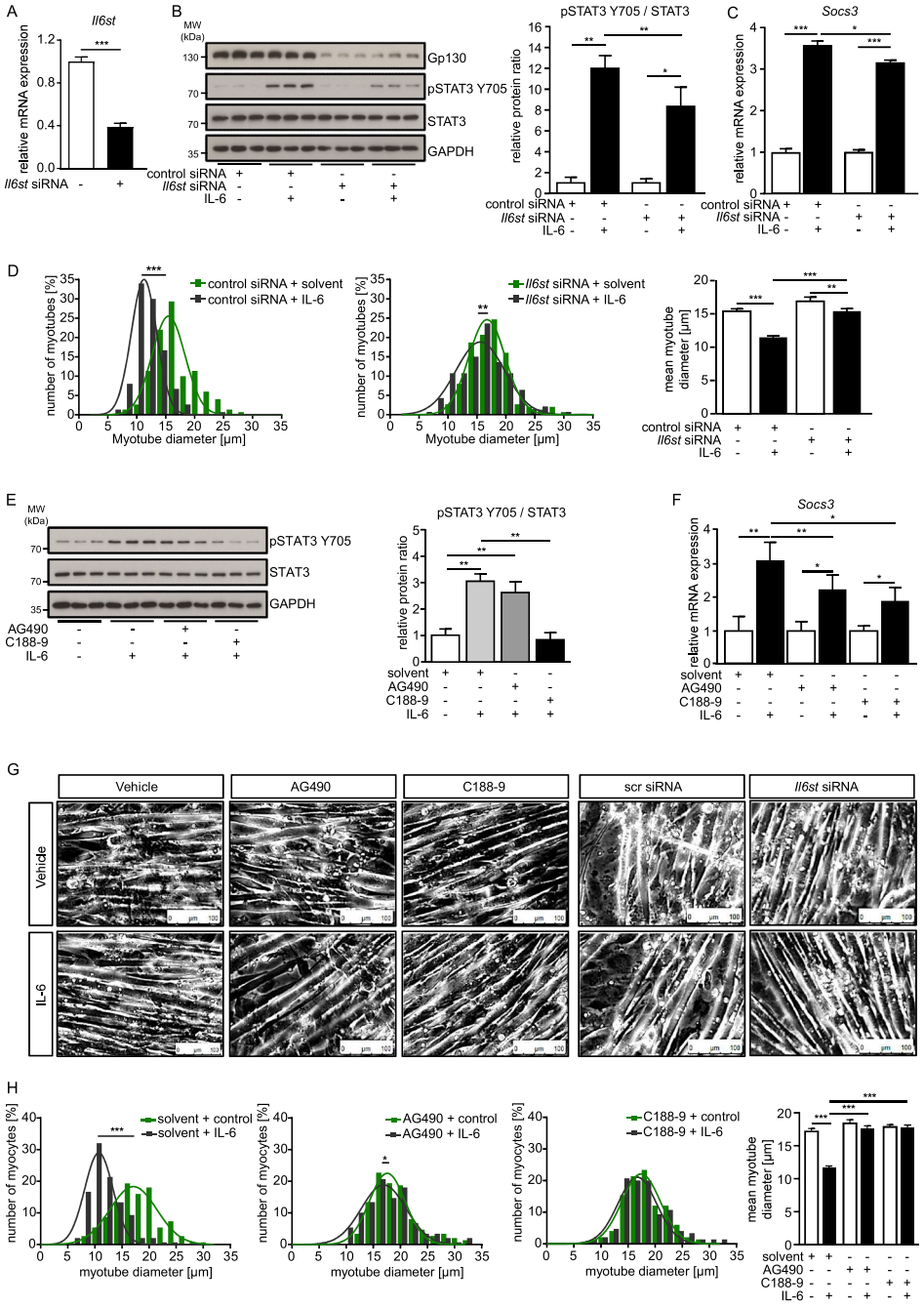

Figure 3 Interleukin 6 mediates atrophy through gp130/JAK2/STAT3 signalling in myocytes. (*A–D*) Five days differentiated C2C12 myotubes were transfected with control siRNA (control siRNA, 50 nM) (*n* = 6) or siRNA targeting Il6st/gp130 (Il6st siRNA, 50 nM) (*n* = 6) followed by treatment with IL-6 (10 ng/mL) or vehicle control, as indicated, for 24 h. (*A*) Quantitative real-time polymerase chain reaction (qRT-PCR) analysis of *Il6st* expression. mRNA expression was normalized to *Gapdh*. (*B*) Western blot analysis with anti-gp130, anti-phospho-STAT3-Tyr705 (pSTAT3 Y705), anti-STAT3, and anti-GAPDH antibodies, *n* = 3. GAPDH was used as loading control. Bar graph showing the ratio of the relative densities of pSTAT3 Y705 and STAT3 protein contents as detected in (*B*). (*C*) qRT-PCR analysis of *Socs3* expression. mRNA expression was normalized to *Gapdh*. (*D*) Frequency distribution histograms of cell width of IL-6 and vehicle-treated myotubes, *n* = 100 cells per condition. Bar graph showing mean myotube width. (*E–H*) Five days differentiated C2C12 myotubes were treated with the JAK2 inhibitor AG490 (*n* = 6), the STAT3 inhibitor C188-9 (*n* = 6) or vehicle control prior to treatment with IL-6 (10 ng/mL) or solvent control, as indicated, for 24 h. (*E*), Western blot analysis with anti-phospho-STAT3-Tyr705 (pSTAT3 Y705), anti-STAT3, and anti-GAPDH antibodies, *n* = 3. GAPDH was used as loading control. Bar graph showing the ratio of the relative densities of pSTAT3 Y705 and STAT3 protein contents as detected (*E*). Data are shown as mean ± SD. (*F*) qRT-PCR analysis of *Socs3* expression. mRNA expression was normalized to *Gapdh*. (*G*) Representative light microscopy pictures. Scale bar = 100 µm. Data are presented as mean ± SD. $^{*}P < 0.05$, $^{**}P < 0.01$, $^{***}P < 0.001$. MW, molecular weight, IL-6, interleukin 6. (*H*) Frequency distribution histograms of cell width of IL-6 and vehicle-treated myotubes in the absence or presence of JAK2 and STAT3 inhibitors, and *Il6st* siRNA or scrambled siRNA control, as indicated, *n* = 100 cells per condition. Bar graph showing mean myotube width.

DOI: 10.1002/jcsm.12867

weight, and IL-6 plasma levels (*Table* S3, *Figure* S7B). Septic WT mice showed an increased STAT3 Y705 phosphorylation in the TA, which was diminished in septic cKO mice 24 h after CLP (*Figure* 4A). *Socs3* expression was increased in the TA of WT CLP, and this increase was attenuated in cKO after 24 h (22-fold vs. 6-fold, $P < 0.01$; *Figure* S8A) and 96 h (22-fold vs. 3.0-fold, $P < 0.001$; *Figure* 4B). These data indicate that gp130 mediates STAT3 activation and *Socs3* expression in TA of septic mice. The observed reduction in TA (WT: −22.3%, cKO: −13.5%; $P < 0.001$; *Figure* 4C) and gastrocnemius/plantaris (GP) weights (WT: −19.7%, cKO: −7.7%; $P < 0.001$; *Figure* 4G, *Table* S3) after 96 h of sepsis, was less pronounced for both muscles in cKO mice ($P < 0.001$ for both). ATPase-stained histological cross sections showed a reduction in MCSA of fast twitch/type II myofibres of septic WT mice that was attenuated in TA (WT: −26.7%, cKO: −6.0%; $P < 0.001$; *Figure* 4D–4F) and GP (WT: −39.1%, cKO: −21.5%; $P < 0.001$; *Figure* 4H–4J) of septic cKO mice. Immunoblotting of muscle protein lysates showed an increase in MuRF1 protein levels in septic WT that was abolished in cKO mice after 24 h (*Figure* S8B) and 96 h (*Figure* 4A). In contrast, we found no differences between the induction of *Trim63* and *Fbxo32*-mRNA expression in TA of WT CLP (*Trim63*: 11.2-fold, $P < 0.01$; *Fbxo32*: 8.2-fold, $P < 0.001$) and cKO CLP mice (*Trim63*: 9-fold, $P < 0.001$; *Fbxo32*: 8.4-fold, $P < 0.001$) after 96 h of sepsis (*Figure* 4K and 4L). Expression of *Myh2*, encoding MyHC2a, was increased in TA of septic cKO but not WT mice when compared with sham animals (*Figure* 4M). In contrast, expression of *Myh4*, encoding MyHC2b, was equally and significantly decreased in TA of WT and cKO mice after 96 h of sepsis (*Figure* 4N). In summary, these data indicate that gp130 activates STAT3/*Socs3* in muscle during sepsis and that *Il6st* deletion prevents sepsis-induced muscle atrophy. This was associated with a reduction of MuRF1 protein levels in cKO mice.

JAK2 inhibition attenuates sepsis-induced muscle atrophy in mice

To investigate the effect of pharmaceutical inhibition of the JAK2/STAT3 pathway, we treated C57BL/6J mice with AG490 or solvent 1 h prior to CLP (AG490: $n = 15$; solvent: $n = 15$) or sham surgery (AG490: $n = 5$; solvent: $n = 5$) and every 24 h until the experimental endpoint at 96 h after surgery. Treatment with AG490 attenuated sepsis-induced STAT3 Y705 phosphorylation ($P < 0.01$, *Figure* 5A) and *Socs3* expression (*Figure* 5B) in TA muscle. AG490 treatment reduced sepsis-induced muscle weight loss (relative reduction 29.6%, $P < 0.05$ in the TA, *Figure* 5C; relative reduction in GP 33.6%, $P < 0.01$, *Figure* 5G, *Table* S4) and reduction in MCSA of fast twitch/type II myofibres (relative reduction 58.3%, $P < 0.001$, in the TA, *Figure* 5D–5F; relative reduction 18.3%, $P < 0.001$ in GP, *Figure* 5H–5J). AG490-treatment attenuated sepsis-induced increase in MuRF1 and Atrogin-1 protein contents (*Figure* 5A). *Trim63* and *Fbxo32* mRNA expression was increased in TA of vehicle-treated CLP mice (CLP vs. sham: *Trim63*: 16.0-fold, $P < 0.01$; *Fbxo32*: 13.4-fold, $P < 0.001$), which was attenuated by AG490 (CLP vs. sham: *Trim63*: 3.0-fold; *Fbxo32*: 3.0-fold; both $P < 0.05$ vs. vehicle CLP) (*Figure* 5K and 5L). Comparable results were obtained in GP muscle (*Figure* S9A–S9D). Neither sepsis nor AG490 treatment had an effect on *Myh2* mRNA expression in TA or GP muscles (*Figure* 5M, *Figure* S9F). In contrast, sepsis decreased *Myh4* mRNA expression in TA and GP, which was attenuated by AG490 treatment (*Figures* 5N and S9G). In summary, these data indicate that JAK2 inhibition attenuates sepsis-induced skeletal muscle atrophy, which coincides with *Trim63*/MuRF1, *Fbxo32*/Atrogin-1 and Myosin expression in mice.

Interleukin 6 interferes with insulin-induced IRS-1/Akt-signalling

RNAseq data from TA of septic WT mice showed a down-regulation of the gene signature of PI3K/Akt signalling (*Figure* S2). Immunoblotting confirmed a decreased Akt S473 phosphorylation in TA of septic WT but not cKO mice (*Figure* 6A). To investigate the interaction between the IL-6 and insulin pathways, we co-treated C2C12 myocytes with IL-6 and insulin. Insulin treatment resulted in increased insulin receptor substrate 1 (IRS-1) S636/639 and Akt S473 phosphorylation, which was blocked by pretreatment with IL-6 (*Figure* 6B). These data indicate that IL-6 inhibits insulin signalling, suggesting that IL-6-induced atrophy is mediated by both an increased protein degradation and a decreased protein synthesis.

Discussion

Our novel findings are as follows. First, the IL-6/gp130/JAK2/STAT3 target gene *SOCS3* was increased in muscle of ICUAW patients when compared with controls. Second, IL-6 caused atrophy of C2C12 myotubes, which was attenuated by knockdown of *Il6st*/gp130 and treatment with JAK2 or STAT3 inhibitors. Third, skeletal muscle specific deletion of *Il6st* and pharmacological JAK2 inhibition by AG490 attenuated sepsis-induced muscle atrophy in mice *in vivo*. Fourth, IL-6 promoted protein degradation and inhibited insulin signalling, which might reduce muscular protein synthesis and therefore protein homeostasis.

Recently, we showed that IL-1β and SAA1 are crucial for muscle atrophy in sepsis and that both increased the mRNA and protein expression of IL-6 as well as MuRF1/*Trim63* and Atrogin-1/*Fbxo32*.[11,12,26] Together with our novel data, we

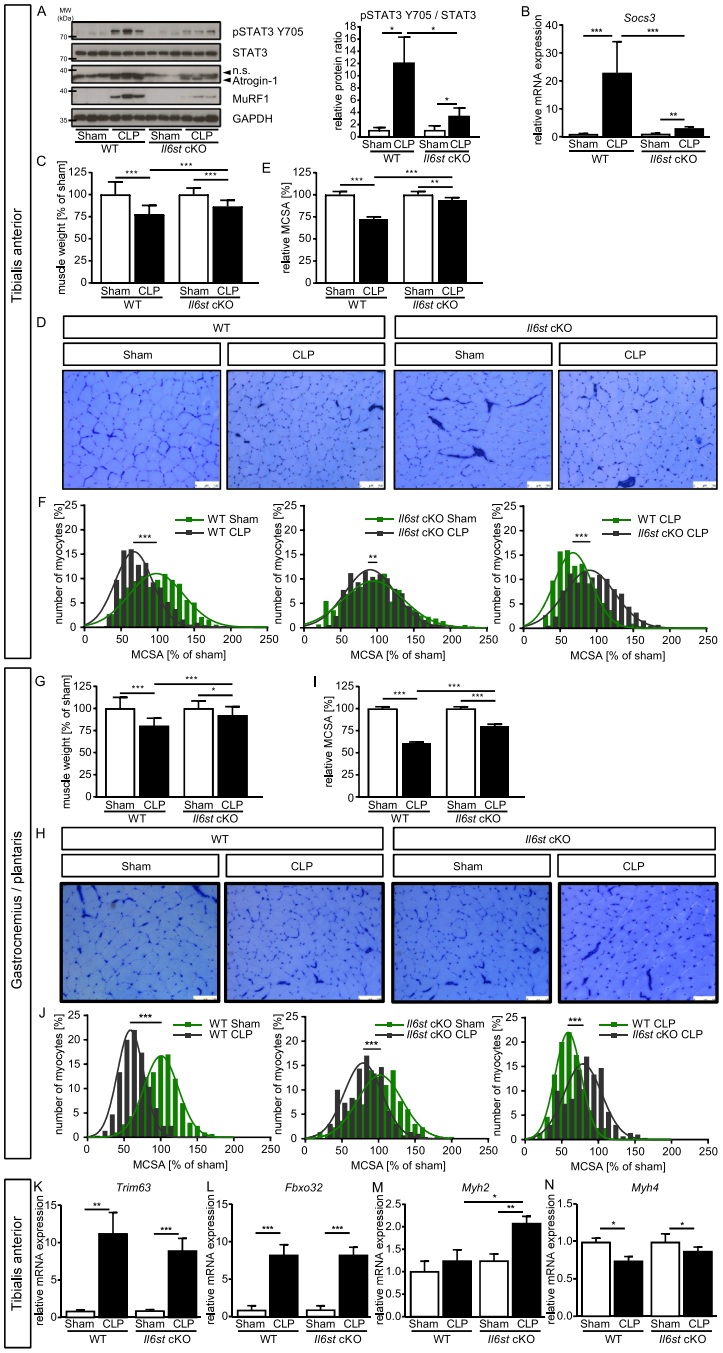

Figure 4 Deletion of *Il6st* in skeletal myocytes attenuates sepsis-induced muscle atrophy in mice. Twelve- to 16-week-old male *Il6st* cKO mice and wildtype (WT) littermates were subjected to cecal ligation and puncture (CLP) or sham surgery. Analyses were performed 24 h (for Western blot: WT sham, $n = 4$; WT CLP, $n = 6$; KO sham, $n = 4$; KO CLP, $n = 4$) or 96 h (for qRT PCR and morphological analyses: WT sham, $n = 6$; WT CLP, $n = 15$; KO sham, $n = 6$; KO CLP, $n = 10$) after surgery in *tibialis anterior* (TA) and *gastrocnemius and plantaris* (GP). (*A*) Western blot analysis with anti-phospho-STAT3-Tyr705 (pSTAT3 Y705), anti-STAT3, anti-Atrogin-1, anti-MuRF1, and anti-GAPDH antibodies, $n = 3$. GAPDH was used as loading control. Bar graph showing the ratio of the relative densities of pSTAT3 Y705 and STAT3 protein contents as detected in (*A*) as mean ± SD. Arrow denotes non-specific (*n*.s.) signal. (*B*) Quantitative real-time polymerase chain reaction (qRT-PCR) analysis of *Socs3*. mRNA expression was normalized to *Gapdh*. Data are presented as mean ± SEM; $^{**}P < 0.01$, $^{***}P < 0.001$. (*C*, *G*) Analyses of TA and GP muscle weights normalized to tibia length of the same animal. (*D*, *H*) Metachromatic ATPase staining of histological cross-sections from TA and GP of sham or CLP operated WT and *Il6st* cKO mice. (*E*, *I*) Mean myofibre cross-sectional area (MCSA) of TA and GP muscle. (*F*, *J*) Frequency distribution histograms of fast/type II MCSA of sham-treated and CLP-treated *Il6st* cKO and WT mice of TA and GP muscle. Data are presented as mean ± SEM; $^{*}P < 0.05$, $^{**}P < 0.01$, $^{***}P < 0.001$. (*K*–*N*) qRT-PCR analysis of *Trim63*, *Fbxo32*, *Myh2*, and *Myh4*. mRNA expression was normalized to *Gapdh*. Data are presented as mean ± SEM; $^{*}P < 0.05$, $^{**}P < 0.01$, $^{***}P < 0.001$.

DOI: 10.1002/jcsm.12867

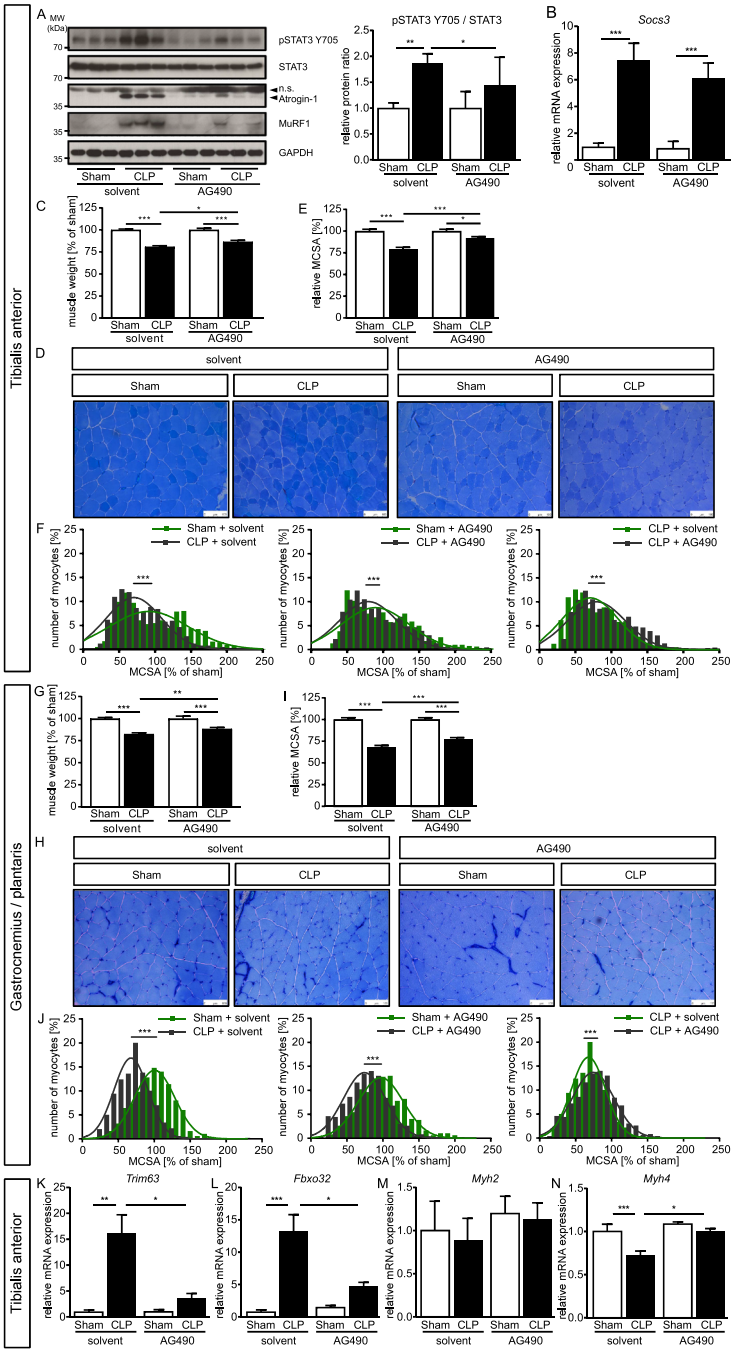

Figure 5 The JAK2 inhibitor AG490 attenuates sepsis-induced muscle atrophy in mice. Twelve- to 16-week-old male *Il6st* cKO and wildtype (WT) mice were treated with the JAK2 inhibitor AG490 (n = 20, 10 μM) or vehicle (n = 20) and then subjected to cecal ligation and puncture (CLP) or sham surgery (solvent sham, n = 5; solvent CLP, n = 15; AG490 sham, n = 5; AG490 CLP, n = 15). Analyses were performed 96 h after surgery in *tibialis anterior* (TA) and *gastrocnemius and plantaris* (GP) of sham-treated and CLP-treated AG490 and vehicle-treated animals. (*A*) Western blot analysis with anti-phospho-STAT3-Tyr705 (pSTAT3 Y705), anti-STAT3, anti-Atrogin-1, anti-MuRF1, and anti-GAPDH antibodies, n = 3. GAPDH was used as loading control. Bar graph showing the ratio of the relative densities of pSTAT3 Y705 and STAT3 protein contents as detected in (*A*) as mean ± SD. Arrow denotes non-specific (n.s.) signal. (*B*) Quantitative real-time polymerase chain reaction (qRT-PCR) analysis of *Socs3*. mRNA expression was normalized to *Gapdh*. Data are presented as mean ± SEM; $^{***}P < 0.001$. (*C*, *G*) Analyses of TA and GP muscle weights normalized to tibia length of the same animal. (*D*, *H*) Metachromatic ATPase staining of histological cross-sections from TA and GP of sham and CLP operated AG490- and solvent-treated mice. (*E*, *I*) Mean myofibre cross-sectional area (MCSA) of TA and GP muscle. (*F*, *J*) Frequency distribution histograms of fast/type II MCSA of sham-operated and CLP-operated AG490-treated and solvent-treated mice. Data are presented as mean ± SEM; $^{*}P < 0.05$, $^{**}P < 0.01$, $^{***}P < 0.001$. (*K*–*N*) Quantitative real-time polymerase chain reaction (qRT-PCR) analysis of *Trim63*, *Fbxo32*, *Myh2*, and *Myh4*. mRNA expression was normalized to *Gapdh*. Data are presented as mean ± SEM; $^{*}P < 0.05$, $^{**}P < 0.01$, $^{***}P < 0.001$.

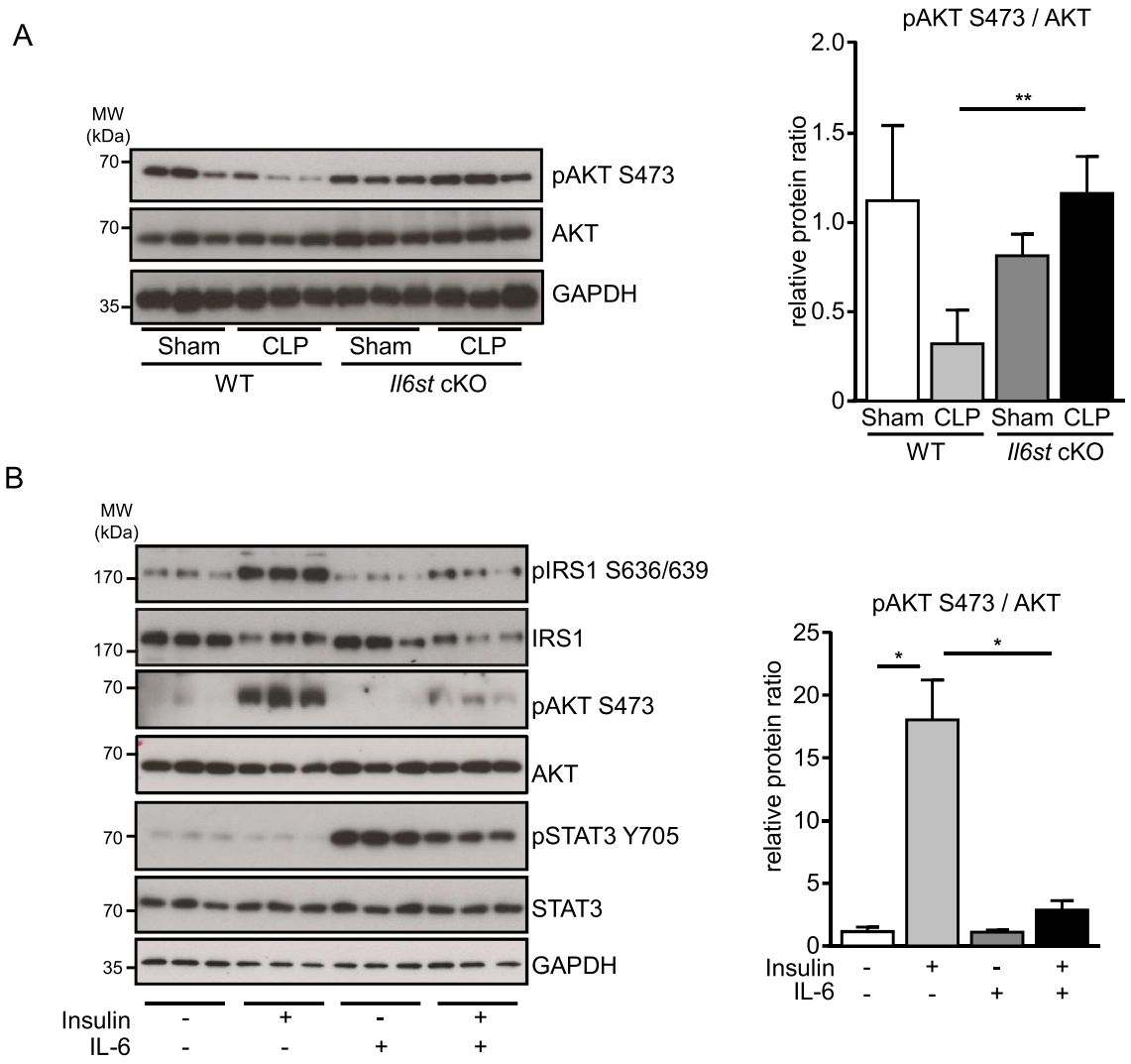

Figure 6 IL-6 inhibits insulin signalling in myocytes *in vitro*. (*A*) Twelve- to 16-week-old male *Il6st* cKO and wildtype (WT) mice were subjected to cecal ligation and puncture (CLP) or sham surgery (WT sham, $n = 4$; WT CLP, $n = 6$; KO sham, $n = 4$; KO CLP, $n = 4$). Analyses were performed 24 h after surgery. Western blot analysis with anti-Akt, anti-pAkt S473, and anti-GAPDH antibodies, $n = 3$. GAPDH was used as loading control. Bar graph showing the ratio of the relative densities of pAkt S473 and Akt protein contents as detected in (*A*) as mean ± SD. (*B*) Five days differentiated C2C12 myotubes were treated with IL-6 (10 ng/mL) or vehicle for 30 min ($n = 6$) before insulin-treatment for 1 h ($n = 3$). Western blot analysis with anti-Akt, anti-pAkt S473, anti-STAT3, anti-pSTAT3 Y705, anti-pIRS1 S636/639, anti-IRS1, and anti-GAPDH antibodies, $n = 3$. GAPDH was used as loading control. Bar graph showing the ratio of the relative densities of pAkt S473 and Akt as well as pSTAT3 Y705 and STAT3 protein contents mean ± SD; $^{*}P < 0.05$, $^{**}P < 0.01$, $^{***}P < 0.001$.

propose that the atrophic effect of IL-1β and SAA1 is partially mediated by IL-6. Our data are in accordance with previous reports showing that gp130 via the JAK/STAT pathway mediates muscle atrophy in a cancer cachexia mouse model.[15,27,28] Specifically, increased IL-6 plasma levels are associated with cachexia in various models of cancer, such as Lewis lung carcinoma, colon cancer, and melanoma. In accordance with our data, STAT3 inhibition attenuated cancer-associated muscle wasting in mice bearing colon-26 carcinoma.[16] Mice devoid of *Il6st* in myocytes were protected from cancer cachexia, which was attributed to a reduced Atrogin-1 expression, while MuRF1 was not analysed.[27] However, compared with this cancer-cachexia model where only mildly elevated IL-6 plasma levels were reported,[27] we measured 10 times higher IL-6 levels in septic mice. In addition, while cancer is a chronic condition, the cytokine storm in sepsis is acute. These differences may explain the different kinetics of muscle wasting that develops gradually in cancer but occurs rapidly in sepsis.

The JAK2 inhibitor AG490 attenuated sepsis-induced muscle atrophy *in vitro* and *in vivo*. This was associated with a reduced *Trim63*/MuRF1 and *Fbxo32*/Atrogin-1 expression. Peña *et al*. showed that AG490 leads to a reduction in TNF plasma levels in septic mice.[29] In addition,

Gyurkovska and Ivanovska found decreased IL-6 and IL-12 plasma levels as well as decreased numbers of T-cells and monocytes in the peritoneal lavage of AG490 treated mice with LPS-induced toxic shock.[30] AG490 treatment protected against liver and lung injury and improved survival in CLP-induced sepsis and LPS-induced toxic shock in mice.[29–31] Therefore, we suggest that the anti-atrophic effects of AG490 are not only mediated by inhibition of muscular gp130 signalling but also by its systemic anti-inflammatory effect. Based on our data, JAK2 inhibition might be useful to treat or prevent muscle atrophy in sepsis. Indeed, different JAK inhibitors received approval for clinical use in patients with polycythemia vera and primary myelofibrosis, in which somatic *JAK2* mutations are common. Treatment with the JAK1/2 inhibitor ruxolitinib resulted in clinical improvements in polycythemia vera and an increased survival in primary myelofibrosis.[32,33] Because of the good tolerability of JAK inhibitors and the improved outcomes of JAK inhibitor-treated septic mice, it seems feasible to investigate their effects in septic patients.

Our RNAseq data revealed an increased expression of genes involved in insulin resistance and a decreased expression of genes involved in insulin signalling, suggesting that insulin resistance also occurs in skeletal muscle of septic mice. Our data presented here indicate that insulin resistance in sepsis occurs at the post-insulin receptor level. IL-6 attenuated insulin-induced IRS-1- and Akt-phosphorylation indicative for insulin resistance. We also found that sepsis-mediated Akt-inactivation was prevented in muscle of cKO mice. This indicates improved insulin signalling and suggests that gp130 signalling contributes to insulin resistance in muscle of septic mice. Our findings are in accordance with previous reports that IL-6 induces insulin resistance in hepatocytes and skeletal muscle cells.[34] However, contradictory results have been reported about the effects of IL-6 on Akt phosphorylation. For example, IL-6 was shown to increase Akt phosphorylation and protein synthesis in muscle and myeloma cells.[34,35] Others showed that the combined treatment of HepG2 cells with insulin and IL-6 had no effect on Akt phosphorylation.[36] These discrepancies could be explained

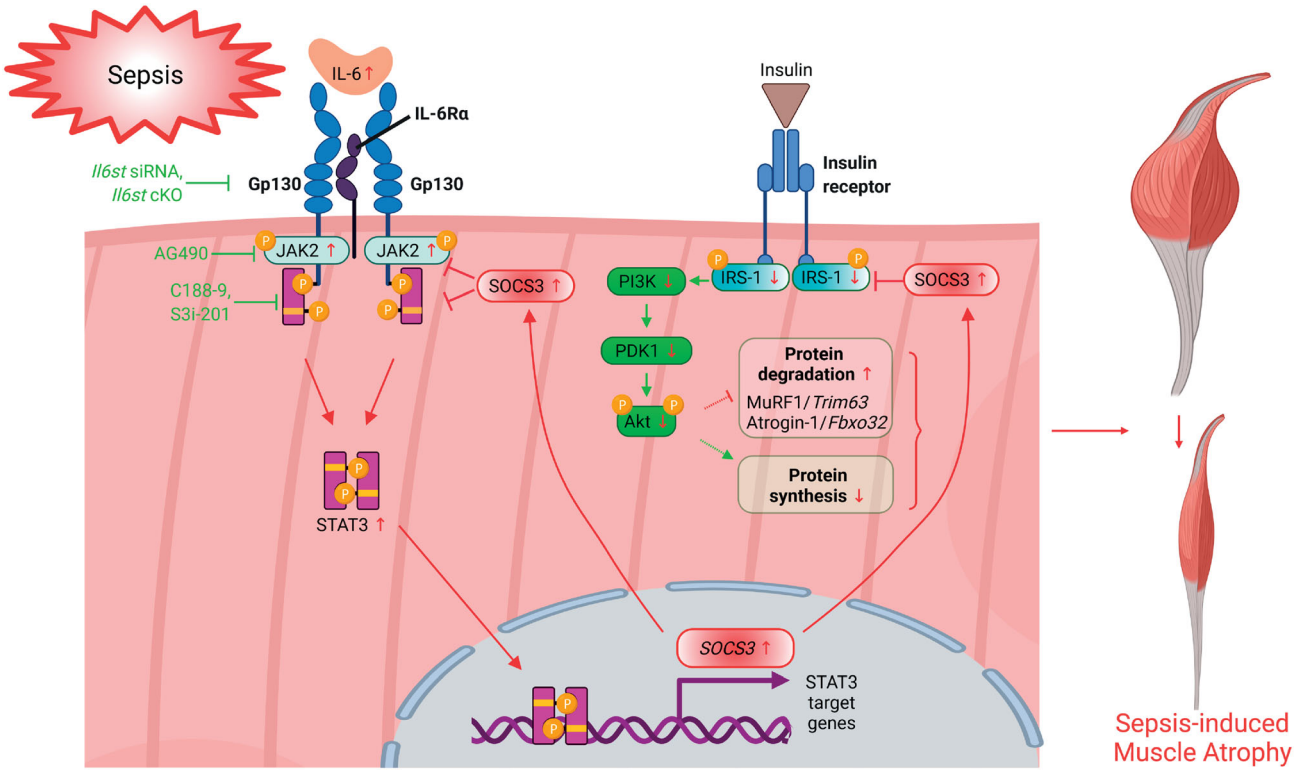

Figure 7 The IL-6/gp130/JAK2/STAT3-pathway mediates sepsis-induced muscle atrophy. IL-6 plasma levels are increased in critically ill human patients and mice with polymicrobial sepsis. IL-6 acts on myocytes via the gp130 and IL-6Rα-complex and activates JAK2- and STAT3-signalling, which leads to an increased expression of *SOCS3*. SOCS3 functions as a negative regulator of cytokine signalling and inhibits the growth promoting insulin/insulin-receptor/Akt pathway by degradation of IRS-1. Reduction of IRS-1 is paralleled by a decreased Akt-activity that results in a reduced protein synthesis and an increased protein degradation, which eventually mediate muscle atrophy. Inhibition of IL-6/gp130 signalling by *Il6st*-knockdown (e.g. *Il6st* siRNA and *Il6st* cKO), JAK2 (e.g. AG490), or STAT3 inhibition (e.g. C188-9 and S3i-201) prevents IL-6-induced *SOCS3* expression as well as myocyte atrophy *in vitro* and skeletal muscle atrophy in vivo. Red arrows indicate changes related to increased IL-6 plasma levels. Fbxo32 indicates F-box protein 32; Gp130, glycoprotein 130; IRS-1, insulin receptor substrate-1; IL-6, interleukin 6; IL-6Rα, interleukin 6 receptor alpha; JAK2, Janus kinase-2; MuRF1, muscle-specific RING finger protein 1; PDK1, 3-phosphoinositide-dependent protein kinase 1; PI3K, phosphatidylinositol 3-kinase; SOCS3, suppressor of cytokine signalling 3; STAT3, signal transducer and activator of transcription 3; Trim63, tripartite motif containing 63. Created with BioRender.com.

by the sensitivity of the model systems, the cell types and the experimental setup used. In our hands, Akt phosphorylation was significantly inhibited in the skeletal muscle of septic mice. In addition, when we preincubated myocytes with IL-6 prior to insulin treatment, insulin-induced IRS-1 and Akt phosphorylation were attenuated, suggesting that IL-6 interferes with insulin signalling in myocytes. Further studies are needed to examine the mechanisms behind IL-6-induced insulin resistance. Based on our data and the body of literature, we conclude that in sepsis, IL-6 via the gp130/JAK2/STAT3/SOCS3 pathway mediates skeletal muscle atrophy by increasing protein degradation and decreasing protein synthesis.

Interestingly, we found a discrepancy between *Trim63* mRNA expression and MuRF1 protein levels in muscle of septic cKO mice. Our data implicate that IL-6 does not increase *Trim63* expression, but possibly increases its translation or its protein stability, or reduces its degradation. Further studies are needed to address this observation.

As a beta-receptor, gp130 is shared by the IL-6 cytokine family consisting of IL-6, IL-11, CNF, LIF, OSM, CT-1, CLCF1, and IL-27.[37] Our RNAseq data showed that the expression of genes involved in IL-6 signalling were increased in muscle of septic mice, whereas the expression of the other IL-6 family members and their receptors was not as much increased or even reduced. Increased IL-6 plasma levels are a risk factor for CIM, and IL-6 strongly induces the JAK/STAT pathway and induces myocyte atrophy *in vitro*. We therefore suggest that IL-6 plays the predominant role among the IL-6 family for sepsis-induced muscle atrophy. However, the involvement of other IL-6 family members in ICUAW warrants further studies.

Conclusion

IL-6 plasma levels are increased in critically ill human patients and mice with polymicrobial sepsis. IL-6 acts on myocytes via the gp130 and IL-6Rα-complex and activates JAK2- and STAT3-signalling, which leads to an increased expression of *SOCS3* (*Figure* 7). SOCS3 functions as a negative regulator of cytokine signalling and inhibits the growth promoting insulin/insulin-receptor/Akt pathway by degradation of IRS-1. Reduction of IRS-1 is paralleled by a decreased Akt-activity that results in a reduced protein synthesis and an increased protein degradation, which eventually mediate muscle atrophy. Inhibition of IL-6/gp130 signalling by *IL6st*-knockdown (e.g. *Il6st* siRNA and *Il6st* cKO), JAK2 (e.g. AG490) or STAT3 inhibition (e.g. C188-9 and S3i-201) prevents IL-6-induced *SOCS3* expression as well as myocyte atrophy in vitro and skeletal muscle atrophy *in vivo* (*Figure* 7). In summary, IL-6 via the gp130/JAK2/STAT3-pathway mediates sepsis-induced muscle atrophy and possibly contributes to ICUAW. An inhibition of this pathway in muscle could be beneficial to prevent sepsis-induced muscle wasting.

Limitations

Our in vitro experiments were performed in murine C2C12 myotubes. Further analyses of primary murine and/or human myocytes are needed to independently confirm our observations about the role of IL-6/gp130/JAK2/STAT3 signalling in myocyte atrophy *in vitro*. In human patients, sepsis frequently occurs at the extremes of ages, especially in elderly patients. Here, we have used 12–20-week-old mice, which relates to a young age in human patients. Although our data are informative for a younger age, further studies on mature (12-month-old) and aged mice (24-month-old) are needed[38] to provide data that are more relevant to the elderly population. Because, we have used only male mice for our experiments, further sex-specific studies are needed to elucidate if IL-6 signalling is equally important for sepsis-induced muscle atrophy in female mice.

Acknowledgements

We thank Claudia Langnick for excellent technical assistance. We are grateful to Klaus Rajewsky for providing the conditional *Il6st* knockout mice, Daniele Sunaga-Franze for help with bioinformatics, and Wei Chen and Bin Zhang for performing RNA sequencing. This study was supported by the *Deutsche Forschungsgemeinschaft* [FI 965/5-1, FI 965/5-2, FI 965/9-1 (to J.F.)] and the German Center for Cardiovascular Research, partner site Greifswald [DZHK 81Z5400153 (to J. F.)] and the Berlin Institute of Health [TRG3-1.2.3 400219 to (J.F., C.B., and S.W.C.)]. The authors of this manuscript certify that they comply with the ethical guidelines for authorship and publishing in the *Journal of Cachexia, Sarcopenia and Muscle*.[39]

Online supplementary material

Additional supporting information may be found online in the Supporting Information section at the end of the article.

Table S1. Primer pairs for genotyping of *Il6st* cKO and *Il6st* WT mice.
Table S2. Primer pairs for quantitative real-time-PCR.
Table S3. Body and organ weights 96 hours after CLP or sham surgery of *Il6st* WT and *Il6st* KO mice
Table S4. Body and organ weights 96 hours after CLP or sham surgery of AG490 and solvent treated WT mice

Figure S1. Differentially expressed genes in muscle of septic mice. Voronoi tree map of differentially expressed genes (**$\log_2$** fold change $\geq$2, adjusted p-value$<$0.05) in TA muscles

of WT mice after 24 (left) or 96 hours (right) after CLP surgery compared to sham treated controls (n = 3 for each condition). Every tile (small polygon) represents one gene. Tiles are arranged and coloured according to the hierarchical KEGG pathway maps (larger regions correspond to functional categories). The diagrams show three hierarchical KEGG pathway levels (top three panels) and the level of individual genes (bottom panel) per time point (24 hours: left panels, 96 hours: right panels). Tile sizes represent changes in gene expression.

Figure S2. Genes up- and downregulated in muscle of septic mice. Significantly up (top) or down (bottom) regulated genes in TA muscle of WT mice 24 (left) or 96 hours (right) after sham or CLP surgery. Analyses for GO-terms and KEGG-pathways are shown (n = 3 for each condition). Data are p-values and presented as $-\log_{10}$

Figure S3. Decreased Genes in muscle of septic mice. Venn Diagram showing the number of genes that were decreased ($\log_2$ fold change $\geq$2, adjusted p-value$<$0.01) in the tibialis anterior muscle of CLP-treated compared to sham treated mice after 24 (left) or 96 hours (right) or at both time points (bottom) (n = 3 for each condition). Data are p-values and presented as $-\log_{10}$.

Figure S4. Regulated genes involved in IL-6 production. Heat map of genes contained in GO:0032635-IL-6 production that were significantly regulated ($p<0.05$) in TA muscle of WT mice 24 hours and 96 hours after CLP or sham surgery (n = 3 for each condition).

Figure S5. Regulated genes involved in JAK-STAT signalling. Heat map of genes contained in GO:0007259-receptor signalling pathway via JAK-STAT that were significantly regulated ($p<0.05$) in TA muscle of WT mice 24 hours and 96 hours after CLP or sham surgery (n = 3 for each condition).

Figure S6. Inhibition of STAT3 attenuates IL-6 induced myotube atrophy *in vitro*. Frequency distribution histograms showing the width of differentiated C2C12 myocytes after 24 hours of treatment with solvent or IL6 after preincubation with DMSO or S3i-201 (n = 100 cells for each condition). Bar graph showing mean myotube width ± SEM. *P $<$0.05 (Student's t-test).

Figure S7. Deletion of *Il6st* in myocytes does not affect interleukin 6 plasma levels in septic mice. (A) Quantitative RT-PCR analysis of Il6st mRNA expression in TA muscle of WT and Il6st cKO mice 96 hours after sham or CLP surgery (WT: Sham n=6, CLP: n=15; cKO: Sham: n=6; CLP: n=10). **(B)** IL-6 plasma concentrations from the same mice. Data information: Data are presented as mean ± SEM. **P $<$0.01, ***P $<$0.001 (Mann-Whitney U test).

Figure S8. Deletion of *Il6st* in myocytes attenuates sepsis-induced *Socs3* expression and MuRF1 protein content. **(A)** Quantitative RT-PCR analysis of Socs3 mRNA content in TA muscle of Il6st cKO and WT mice 96 hours after CLP or sham operation (WT Sham, n=6; WT CLP, n=15; KO Sham, n=6; KO CLP, n=10). Data are presented as mean ± SEM **P $<$ 0.01, ***P $<$ 0.001 (Mann-Whitney U test). **(B)** Immunoblots with anti-Atrogin-1, anti-MuRF1 and anti-GAPDH antibodies in TA muscle of Il6st cKO and WT mice 24 hours after CLP or sham operation (n = 3 for each condition).

Figure S9. Inhibition of JAK2 attenuates sepsis-induced *Socs3* and *Trim63* expression and MuRF1 protein content in gastrocnemius and plantaris muscle. (A) Immunoblots with anti-pSTAT3 Y705, anti-STAT3, anti-Atrogin-1, anti-MuRF1 and anti-GAPDH antibodies in GP muscle of AG490 or solvent treated WT mice 96 hours after CLP or sham surgery (n = 3 for each condition). Bar graph showing the ratio of the relative densities of pSTAT3 Y705 and STAT3 protein contents as detected in B. B-F Quantitative RT-PCR analysis of *Socs3* **(B)**, *Trim63* **(C)**, *Fbxo32* **(D)**, *Myh2* **(E)** and *Myh4* **(F)** mRNA expression in GP muscle of AG490 or solvent treated WT mice 96 hours after CLP or sham surgery (AG490: sham: n=5, CLP: n=15; solvent: sham: n=5, CLP: n=15). Data information: (B-F) Data are presented as mean ± SEM. *P $<$ 0.05, **P $<$ 0.01 (Mann-Whitney U test).

Conflict of interest

Lukas Zanders, Melanie Kny, Alexander Hahn, Sibylle Schmidt, Sebastian Wundersitz, Mihail Todiras, Ines Lahmann, Arnab Bandyopadhyay, Tobias Wollersheim, Lars Kaderali, Friedrich C. Luft, Carmen Birchmeier, Steffen Weber-Carstens, and Jens Fielitz declare that they have no conflict of interest.

References

1. Ali NA, O'Brien JM Jr, Hoffmann SP, Phillips G, Garland A, Finley JC, et al. Acquired weakness, handgrip strength, and mortality in critically ill patients. *Am J Respir Crit Care Med* 2008;**178**:261–268.
2. Sharshar T, Bastuji-Garin S, Stevens RD, Durand MC, Malissin I, Rodriguez P, et al. Presence and severity of intensive care unit-acquired paresis at time of awakening are associated with increased intensive care unit and hospital mortality. *Crit Care Med* 2009;**37**:3047–3053.
3. Herridge MS, Tansey CM, Matte A, Tomlinson G, Diaz-Granados N, Cooper A, et al. Functional disability 5 years after acute respiratory distress syndrome. *N Engl J Med* 2011;**364**:1293–1304.
4. Wollersheim T, Woehlecke J, Krebs M, Hamati J, Lodka D, Luther-Schroeder A, et al. Dynamics of myosin degradation in intensive care unit-acquired weakness

during severe critical illness. *Intensive Care Med* 2014;**40**:528–538.
5. Puthucheary ZA, Rawal J, McPhail M, Connolly B, Ratnayake G, Chan P, et al. Acute skeletal muscle wasting in critical illness. *JAMA* 2013;**310**:1591–1600.
6. Bierbrauer J, Koch S, Olbricht C, Hamati J, Lodka D, Schneider J, et al. Early type II fiber atrophy in intensive care unit patients with nonexcitable muscle membrane. *Crit Care Med* 2012;**40**:647–650.
7. Bodine SC, Latres E, Baumhueter S, Lai VK, Nunez L, Clarke BA, et al. Identification of ubiquitin ligases required for skeletal muscle atrophy. *Science* 2001;**294**:1704–1708.
8. Weber-Carstens S, Deja M, Koch S, Spranger J, Bubser F, Wernecke KD, et al. Risk factors in critical illness myopathy during the early course of critical illness: a prospective observational study. *Crit Care* 2010;**14**:R119.
9. Winkelman C. The role of inflammation in ICU-acquired weakness. *Crit Care* 2010;**14**: 186.
10. Huang N, Kny M, Riediger F, Busch K, Schmidt S, Luft FC, et al. Deletion of Nlrp3 protects from inflammation-induced skeletal muscle atrophy. *Intensive Care Med Exp* 2017;**5**:3.
11. Langhans C, Weber-Carstens S, Schmidt F, Hamati J, Kny M, Zhu X, et al. Inflammation-induced acute phase response in skeletal muscle and critical illness myopathy. *PLoS One.* 2014;**9**:e92048, https://doi.org/10.1371/journal.pone.0092048
12. Hahn A, Kny M, Pablo-Tortola C, Todiras M, Willenbrock M, Schmidt S, et al. Serum amyloid A1 mediates myotube atrophy via Toll-like receptors. *J Cachexia Sarcopenia Muscle* 2020;**11**:103–119.
13. Tierney MT, Aydogdu T, Sala D, Malecova B, Gatto S, Puri PL, et al. STAT3 signaling controls satellite cell expansion and skeletal muscle repair. *Nat Med* 2014;**20**: 1182–1186.
14. Hoene M, Runge H, Haring HU, Schleicher ED, Weigert C. Interleukin-6 promotes myogenic differentiation of mouse skeletal muscle cells: role of the STAT3 pathway. *Am J Physiol Cell Physiol* 2013;**304**:C128–C136.
15. Bonetto A, Aydogdu T, Kunzevitzky N, Guttridge DC, Khuri S, Koniaris LG, et al. STAT3 activation in skeletal muscle links muscle wasting and the acute phase response in cancer cachexia. *PLoS One* 2011;**6**:e22538, https://doi.org/10.1371/journal.pone.0022538
16. Bonetto A, Aydogdu T, Jin X, Zhang Z, Zhan R, Puzis L, et al. JAK/STAT3 pathway inhibition blocks skeletal muscle wasting downstream of IL-6 and in experimental cancer cachexia. *Am J Physiol Endocrinol Metab* 2012;**303**:E410–E421.
17. Wen Z, Zhong Z, Darnell JE Jr. Maximal activation of transcription by Stat1 and Stat3 requires both tyrosine and serine phosphorylation. *Cell* 1995;**82**:241–250.
18. Heinrich PC, Behrmann I, Muller-Newen G, Schaper F, Graeve L. Interleukin-6-type cytokine signalling through the gp130/Jak/STAT pathway. *Biochem J* 1998;**334**: 297–314.
19. Babon JJ, Kershaw NJ, Murphy JM, Varghese LN, Laktyushin A, Young SN, et al. Suppression of cytokine signaling by SOCS3: characterization of the mode of inhibition and the basis of its specificity. *Immunity* 2012;**36**:239–250.
20. Rui L, Yuan M, Frantz D, Shoelson S, White MF. SOCS-1 and SOCS-3 block insulin signaling by ubiquitin-mediated degradation of IRS1 and IRS2. *J Biol Chem* 2002;**277**: 42394–42398.
21. Rommel C, Bodine SC, Clarke BA, Rossman R, Nunez L, Stitt TN, et al. Mediation of IGF-1-induced skeletal myotube hypertrophy by PI(3)K/Akt/mTOR and PI(3)K/Akt/GSK3 pathways. *Nat Cell Biol* 2001;**3**:1009–1013.
22. Yoshida T, Delafontaine P. Mechanisms of IGF-1-mediated regulation of skeletal muscle hypertrophy and atrophy. *Cells* 2020; **9**:1970, https://doi.org/10.3390/cells9091970
23. Weber-Carstens S, Schneider J, Wollersheim T, Assmann A, Bierbrauer J, Marg A, et al. Critical illness myopathy and GLUT4: significance of insulin and muscle contraction. *Am J Respir Crit Care Med* 2013;**187**:387–396.
24. Betz UA, Bloch W, van den Broek M, Yoshida K, Taga T, Kishimoto T, et al. Postnatally induced inactivation of gp130 in mice results in neurological, cardiac, hematopoietic, immunological, hepatic, and pulmonary defects. *J Exp Med* 1998;**188**: 1955–1965.
25. Busch K, Kny M, Huang N, Klassert TE, Stock M, Hahn A, et al. Inhibition of the NLRP3/IL-1beta axis protects against sepsis-induced cardiomyopathy. *J Cachexia Sarcopenia Muscle* 2021;https://doi.org/10.1002/jcsm.12763
26. Haberecht-Muller S, Kruger E, Fielitz J. Out of control: the role of the ubiquitin proteasome system in skeletal muscle during inflammation. *Biomolecules* 2021;**11**:1327, https://doi.org/10.3390/biom11091327
27. Puppa MJ, Gao S, Narsale AA, Carson JA. Skeletal muscle glycoprotein 130's role in Lewis lung carcinoma-induced cachexia. *FASEB J* 2014;**28**:998–1009.
28. Silva KA, Dong J, Dong Y, Dong Y, Schor N, Tweardy DJ, et al. Inhibition of Stat3 activation suppresses caspase-3 and the ubiquitin-proteasome system, leading to preservation of muscle mass in cancer cachexia. *J Biol Chem* 2015;**290**: 11177–11187.
29. Peña G, Cai B, Deitch EA, Ulloa L. JAK2 inhibition prevents innate immune responses and rescues animals from sepsis. *J Mol Med (Berl)* 2010;**88**:851–859.
30. Gyurkovska V, Ivanovska N. Tyrosine kinase inhibitor tyrphostin AG490 reduces liver injury in LPS-induced shock. *Eur J Pharmacol* 2015;**751**:118–126.
31. Hui L, Yao Y, Wang S, Yu Y, Dong N, Li H, et al. Inhibition of Janus kinase 2 and signal transduction and activator of transcription 3 protect against cecal ligation and puncture-induced multiple organ damage and mortality. *J Trauma* 2009;**66**: 859–865.
32. Vannucchi AM. Ruxolitinib versus standard therapy for the treatment of polycythemia vera. *N Engl J Med* 2015;**372**:1670–1671.
33. Verstovsek S, Gotlib J, Mesa RA, Vannucchi AM, Kiladjian JJ, Cervantes F, et al. Long-term survival in patients treated with ruxolitinib for myelofibrosis: COMFORT-I and -II pooled analyses. *J Hematol Oncol* 2017;**10**:156.
34. Hideshima T, Nakamura N, Chauhan D, Anderson KC. Biologic sequelae of interleukin-6 induced PI3-K/Akt signaling in multiple myeloma. *Oncogene* 2001;**20**:5991–6000.
35. Gao S, Durstine JL, Koh HJ, Carver WE, Frizzell N, Carson JA. Acute myotube protein synthesis regulation by IL-6-related cytokines. *Am J Physiol Cell Physiol* 2017;**313**: C487–C500.
36. Kortylewski M, Feld F, Kruger KD, Bahrenberg G, Roth RA, Joost HG, et al. Akt modulates STAT3-mediated gene expression through a FKHR (FOXO1a)-dependent mechanism. *J Biol Chem* 2003;**278**: 5242–5249.
37. Tanaka T, Narazaki M, Kishimoto T. IL-6 in inflammation, immunity, and disease. *Cold Spring Harb Perspect Biol* 2014;**6**:a016295, https://doi.org/10.1101/cshperspect.a016295
38. Turnbull IR, Wlzorek JJ, Osborne D, Hotchkiss RS, Coopersmith CM, Buchman TG. Effects of age on mortality and antibiotic efficacy in cecal ligation and puncture. *Shock* 2003;**19**:310–313.
39. von Haehling S, Morley JE, Coats AJS, Anker SD. Ethical guidelines for publishing in the *Journal of Cachexia, Sarcopenia and Muscle*: update 2017. *J Cachexia Sarcopenia Muscle* 2019;**10**:1143–1145.